

# Spatial distribution of Galactic HII regions

R. Paladini<sup>1\*</sup>, R. D. Davies<sup>2†</sup>, G. DeZotti<sup>3‡</sup>

<sup>1</sup>*SISSA, International School for Advanced Studies, via Beirut 2-4, I-34014 Trieste, Italy*

<sup>2</sup>*University of Manchester, Jodrell Bank Observatory, Macclesfield - Cheshire SK11 9DL, UK*

<sup>3</sup>*INAF-Osservatorio Astronomico di Padova, Vicolo dell'Osservatorio 5, I-35122 Padova, Italy*

7 September 2018

## ABSTRACT

We present a new, detailed, analysis of the spatial distribution of Galactic HII regions, exploiting a far richer database than used in previous analyses. Galactocentric distances have been derived for 550 objects. Distances from the Sun could be unambiguously derived from velocity data for 117 of them, lying either outside the solar circle (84) or on a line-of-sight tangential to their orbit (33). For 177 further sources, distance estimates are made possible by the use of auxiliary data. A highly significant correlation between luminosity and linear diameter was found and the corresponding least-square linear relationship in the log-log plane was used to resolve the distance ambiguity for an additional 256 sources. Within the solar circle the thickness of the distribution of HII regions around the Galactic plane was found to be comparable to that of OB stars (Bronfman et al. 2000). At larger galactocentric radii the shape of the distribution reflects that of the warp, and its thickness along the  $z$  axis increases with increasing distance from the Galactic centre. We also confirm, for a much larger sample, the previously reported positive gradient of electron temperature with galactocentric distance.

**Key words:** HII regions – Galaxy: structure – radio continuum: ISM

## 1 INTRODUCTION

As it is well known, HII regions are among the most reliable tracers of the Galactic spiral structure (Vallée 1995). The reconstruction of their spatial distribution is also important for understanding the distribution of free electrons (Taylor & Cordes 1993; Cordes & Lazio 2002, 2003). Recovering such a distribution, however, is complicated by the distance degeneracy problem. While the galactocentric distances can be derived from the Galactic rotation curve if velocity data are available, there are in general two solutions (“near” and “far”) for the distance from the Sun of regions within the solar circle.

In this paper we exploit the rich information content of the extensive radio catalog of Galactic HII regions published by Paladini et al. (2003, hereafter Paper I) to address this problem. The paper is organized as follows. In Sect. 2 we briefly describe the catalog and analyze its completeness. In Sect. 3 we describe the derivation of galactocentric distances and investigate the radial gradient of the electron temperature, discovered in previously published works. In Sect. 4 we discuss distances from the Sun and methods to overcome the

degeneracy; the thickness of the HII layer is also estimated. The main conclusions are summarized in Sect. 5.

## 2 THE CATALOG

### 2.1 Description

The extensive radio catalog of Galactic HII regions, presented in Paper I, has been produced by exploiting the data contained in 24 previously published lists (see Table 1 in Paper I for details and references). The final compilation - the so-called Master Catalog - includes 1442 classical HII regions (i.e., bright, compact objects) for which original flux densities and diameters as well as the available information on line velocities, line widths and line temperatures and the errors on these quantities are listed. The catalog does not include ultra-compact (UCHII) and extremely extended (EHE) sources.

A Synthetic Catalog of flux densities and diameters at 2.7 GHz (with the corresponding errors) for each of the 1442 sources of the Master Catalog has also been produced. When not directly available, the flux density - and the corresponding error - at 2.7 GHz has been computed by extrapolating/interpolating the published observational data at other frequencies. For sources lacking a measurement of the angular diameter (14% of the total), an indicative diameter has

\* E-mail: paladini@sissa.it

† E-mail: rdd@jb.man.ac.uk

‡ E-mail: dezotti@pd.astro.it

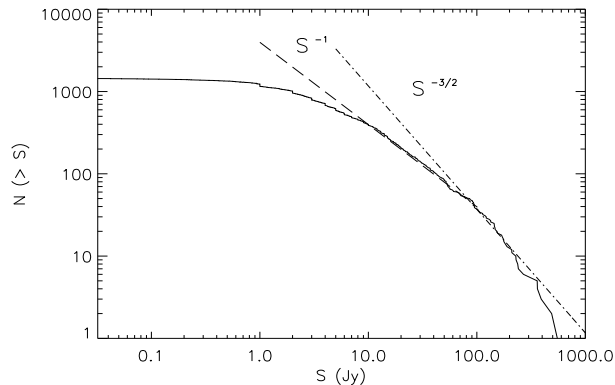


**Figure 1.** Cumulative counts  $N(> S)$  of HII regions in the catalog by Paladini et al. (2003).

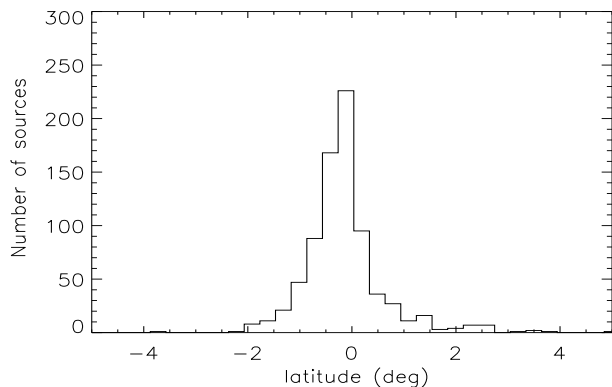


**Figure 2.** Galactic latitude distribution of  $\simeq 800$  sources with detection of recombination lines.

been estimated, based on the observed angular diameter - flux density correlation (see Paper I for more details).

## 2.2 Completeness of the catalog

As shown by Fig. 1, the bright tail ( $300 \text{ Jy} \gtrsim S_{2.7\text{GHz}} \gtrsim 70 \text{ Jy}$ ) of the integral counts,  $N(> S)$ , of HII regions listed in Paper I exhibits the Euclidean slope [ $N(> S) \propto S^{-3/2}$ ] as expected for the nearest sources (within a distance not exceeding the thickness of the HII layer). At fainter fluxes the counts flatten to  $N(> S) \propto S^{-1}$ , consistent with the 2-D (disk-like) distribution of more distant sources. Below  $\simeq 7 \text{ Jy}$  the counts become still flatter, suggesting the onset of a substantial incompleteness.

The completeness limit is to a large extent determined by source confusion. The surface density of catalogued sources reaches values of one source per few beams in the region  $\pm 60^\circ$  around  $l = 0^\circ$ ,  $b \sim 0^\circ$ , for a typical  $10'$  beam. As extensively discussed in the literature (e.g., Scheuer 1957; Condon 1974; Hogg 2001) confusion becomes important at flux levels at which there are more than  $1/30$  sources per beam. Correspondingly, it is very difficult to resolve into individual sources the structure seen right in the Galactic plane, particularly towards the Galactic center. Thus, the majority of weak HII regions are actually found in less crowded areas, such as the anti-center region or regions at  $|b| > 1^\circ$ .

**Table 1.** References for velocity data.

Reference	Line
Caswell & Haynes 1987	H109 $\alpha$ /H110 $\alpha$
Downes et al. 1980	H110 $\alpha$
Lockman 1989	H85 $\alpha$ /H87 $\alpha$ /H88 $\alpha$
Reifenstein et al. 1970	H109 $\alpha$
Wilson et al. 1970	H109 $\alpha$
Wink et al. 1982	H76 $\alpha$ /H90 $\alpha$
Wink et al. 1983	H76 $\alpha$

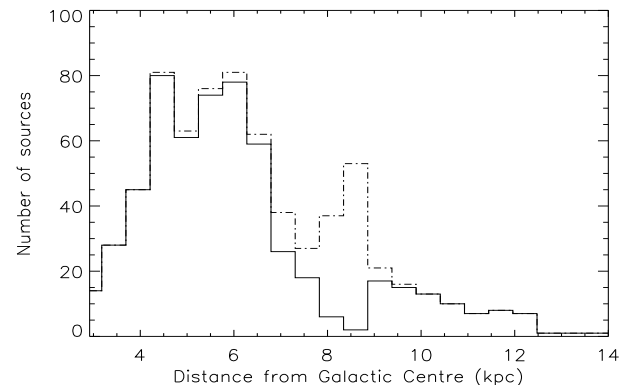


**Figure 3.** Distribution of galactocentric distances of all  $\simeq 800$  sources with velocity data (dashed line). The solid line shows the distribution of 575 sources with radial velocities  $|V_r| > 10 \text{ km s}^{-1}$ .

## 3 GALACTOCENTRIC DISTANCES OF HII REGIONS

### 3.1 Distance estimates

Paper I contains radio recombination line velocities for  $\simeq 800$  of the catalogued HII regions. The references for the velocity data and the lines used are listed in Table 1. This is, by far, the largest sample used to derive distances. The present analysis also improves on the earlier ones because of the adoption of an updated Galaxy rotation curve. Previous studies (Caswell & Haynes 1987; Downes et al. 1980) were based on  $\simeq 300$  sources and used Schmidt's (1965) rotation curve or slightly modified versions of it.

The rotation velocity  $\Theta$  around the Galactic centre of an object at galactocentric distance  $R$ , Galactic longitude  $l$ , and with radial velocity  $V_r$  in the local standard of rest, is given by:

$$\Theta = (R/R_0)(\Theta_0 + V_r/\sin l) \quad (1)$$

where  $\Theta_0$  and  $R_0$  denote, respectively, the rotation velocity and the galactocentric distance of the Sun. We adopt the IAU-recommended values of  $R_0 = 8.5 \text{ kpc}$  and  $\Theta_0 = 220 \text{ km s}^{-1}$  (Kerr & Lynden-Bell 1986). From Eq. (1) we can derive  $R$  from radial velocity measurements, if the rotation curve  $\Theta(R)$  is known. We have used the linear expression derived by Fich, Blitz and Stark (1989) (hereafter FBS89), holding for galactocentric distances between 3 and 17 kpc:

$$\Theta = (221.64 - 0.44R) \text{ km s}^{-1} \quad (2)$$

where  $R$  is in kpc.

The outer part of the FBS89 rotation curve was con-

structured using HII regions spectrophotometric distances and velocities. Our sample has some sources in common with theirs, namely those with CO velocity measurements. To avoid circularity we have excluded such sources from further analysis. Thus the velocity measurements we have used are fully independent of those used by FBS89. As discussed by Blitz (1979) and FBS89, the use of HII regions to derive a rotation curve yields relatively small absolute errors compared with methods relying on other classes of objects such as star clusters, planetary nebulae, carbon stars, and diffuse atomic hydrogen. On the other hand, the good agreement of the FBS89 rotation curve with determinations using other methods indicates that systematic errors specific to HII regions cannot be large except, perhaps, in specific regions where systematic, non-circular, velocity components (e.g. streaming motions) are present. One such region is the Perseus arm where a mean streaming velocity  $\simeq 12 \text{ km sec}^{-1}$  has been found by Brand & Blitz (1993). As a consequence, the distances of 36 sources in that region may be affected by a substantial systematic error.

The mean measurement error on  $V_r$  is  $\simeq 1 \text{ km s}^{-1}$ , although with a large scatter (the minimum error is  $0.02 \text{ km s}^{-1}$ ; the maximum  $10.7 \text{ km s}^{-1}$ ). The corresponding error on the derived values of  $R$  are typically of order 1%. On the other hand, random motions can add a significant uncertainty to the computed values of  $R$ . The average local peculiar velocities reported by Stark & Brand (1989) and Clemens (1985) are  $\simeq 5 \text{ km s}^{-1}$ . To curtail this effect, we consider only objects with  $|V_r| \geq 10 \text{ km s}^{-1}$ . As a consequence, we are left with 575 sources.

The distribution of the derived galactocentric distances is shown in Fig. 3, where the peaks corresponding to the spiral arms at  $R = 4, 6$  and  $8 \text{ kpc}$  are visible. The latter peak, due to sources on or near the solar circle, however disappears if we consider only sources with  $|V_r| \geq 10 \text{ km s}^{-1}$ .

### 3.2 Electron temperature vs Galactocentric distance

We are now in a position to investigate the dependence of HII region electron temperatures upon Galactocentric distance. For 404 of the 575 sources with more reliable estimates of  $R$ , electron temperatures,  $T_e$ , are available (Caswell & Haynes 1987; Downes et al. 1980; Reifenstein et al. 1970; Wilson et al. 1970; Wink et al. 1982, 1983) and listed in Paper I. Non-LTE effects should be small over the entire range of frequencies 5 to 22 GHz (Shaver et al. 1983; Wink et al. 1983), so that corrections to the computed  $T_e$  values are not necessary. When two or more values of  $T_e$  are available for the same source, their weighted average has been taken. The data shown in Fig. 4 confirm the previously reported correlation between  $T_e$  and  $R$ , based on much smaller samples (Churchwell et al. 1978; Downes et al. 1980; Shaver et al. 1983). The least-square linear relationship is:

$$T_e = (4166 \pm 124) + (314 \pm 20)R \quad \text{K} \quad (3)$$

close to the previous result by Shaver et al. (1983) who found  $T_e = (3150 \pm 110) + (433 \pm 40)R \quad \text{K}$ .

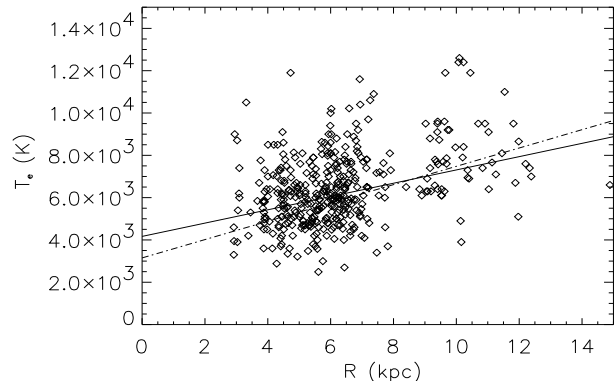


**Figure 4.** Electron temperatures versus galactocentric distance. The solid line shows our least-squares linear relationship, the dot-dashed line that found by Shaver et al. (1983).

## 4 DISTANCES FROM THE SUN

The galactocentric radius  $R$  is related to the distance  $D$  from the Sun by the equation:

$$R = (R_0^2 + D^2 - 2DR_0 \cos l)^{\frac{1}{2}}, \quad (4)$$

which has obviously, in general, two real solutions for  $D$  if  $R \leq R_0$ :

$$D_{far/near} = R_0(\cos l \pm (\cos^2 l - (1 - (R/R_0)^2))^{\frac{1}{2}}) \quad (5)$$

corresponding to the two intersections of the line-of-sight with the orbit of radius  $R$ . The solution is unique only for sources lying outside the solar circle or whose line-of-sight is tangent to their orbit.

To break the degeneracy we need auxiliary data. Two kinds of data have been used: absorption lines and optical counterparts. Since only neutral (HI) or molecular ( $\text{H}_2\text{CO}$  and OH) gas in front of an HII region can absorb its continuum emission, if the region is at the “near” distance the gas absorption line velocity is lower than its recombination line velocity. On the other hand, if the HII region is at the “far” distance it is possible to detect absorption at a velocity higher than that of its recombination line. At the same time, if an optical counterpart is detected, then it is very likely that the HII region is at the “near” distance since the heavy dust obscuration at optical wavelengths makes detections of far sources quite difficult.

Table 2 lists the sources for which the ambiguity can be resolved using auxiliary data. HI data are mainly taken from Kuchar & Bania (1994) and Caswell et al. (1975). Additional data are taken from Kerr & Knapp (1970) and Goss & Radhakrishnan (1969).  $\text{H}_2\text{CO}$  data are from Wilson (1980). Optical identifications are from the catalogs by Marsáková (1974), Blitz et al. (1982), and Brand & Blitz (1993). Complementary data on individual sources are from Miller (1968) and Shaver et al. (1981).

Of our 575 sources with  $|V_r| \geq 10 \text{ km s}^{-1}$ , 117 have a unique solution for  $D$  (84 lie outside the solar circle and for 33 the line of sight is tangent to their galactocentric orbit); for 177 others we have additional data allowing us to discriminate between the two solutions; 281 are left with the distance degeneracy. For the latter, we need an additional distance indicator.

**Table 2.** Galactic HII regions for which the distance ambiguity was resolved using auxiliary data. The (o) denotes HII regions with an optical counterpart, for which the “near” solution was chosen; (a1) and (a2) denote sources for which, respectively, HI or H<sub>2</sub>CO absorption data are available.

<i>l</i>	<i>b</i>	<i>Near or Far</i> <i>kinematic distance</i>		<i>l</i>	<i>b</i>	<i>Near or Far</i> <i>kinematic distance</i>		<i>l</i>	<i>b</i>	<i>Near or Far</i> <i>kinematic distance</i>	
6.4	-0.5	near	(o)	25.3	0.3	near	(o)	44.3	0.1	near	(a1)
6.5	0.1	near	(a1)	25.4	-0.3	far	(a2)	45.1	0.1	far	(a1)
6.6	-0.3	near	(o)	25.4	-0.2	far	(a2)	45.5	0.1	far	(a1)
6.6	-0.1	near	(a1)	25.7	0.0	far	(a2)	46.5	-0.2	near	(a1)
6.7	-0.2	near	(a1)	25.8	0.2	tangent	(a2)	48.6	0.0	far	(a1)
7.0	-0.2	near	(o)	26.1	-0.1	far	(a2)	48.6	0.2	far	(a1)
8.4	-0.3	near	(a2)	27.3	0.1	far	(a2)	49.4	-0.2	far	(a1)
8.7	-0.4	near	(o)	27.5	0.2	far	(a2)	51.1	0.2	far	(a1)
10.5	0.0	near	(a2)	28.6	0.0	far	(a2)	52.8	0.3	far	(a1)
11.7	-1.7	near	(o)	28.7	0.0	far	(a2)	53.6	0.0	near	(o)
12.4	-1.1	near	(o)	28.8	0.2	tangent	(a2)	53.6	0.2	far	(a1)
13.4	0.1	far	(a2)	29.0	-0.6	near	(o)	60.9	-0.1	near	(o)
14.0	-0.1	near	(a2)	29.1	-0.7	near	(o)	62.9	0.1	near	(o)
14.2	-0.2	near	(o)	29.9	-0.0	far	(a2)	63.2	0.4	near	(o)
14.2	-0.1	near	(o)	30.2	-0.1	far	(a2)	63.2	0.5	near	(o)
14.4	-0.7	near	(a2)	30.5	0.0	near	(o)	302.8	1.3	near	(o)
14.6	0.0	near	(o)	30.5	0.4	near	(o)	305.4	0.2	far	(a1)
14.6	0.1	near	(a2)	30.6	-0.1	tangent	(a1)	308.7	0.6	near	(o)
15.0	-0.7	near	(o)	30.7	-0.3	tangent	(a2)	311.0	0.4	near	(o)
15.1	-0.9	near	(o)	30.8	-0.0	near	(a1)	311.9	0.1	far	(a1)
15.1	-0.7	near	(o)	31.0	0.0	far	(a1)	311.9	0.2	far	(a1)
15.2	-0.8	near	(a2)	31.2	-0.1	far	(a1)	316.8	-0.1	near	(o)
15.2	-0.6	near	(a2)	31.3	0.1	tangent	(a1)	316.8	-0.0	near	(o)
16.6	-0.3	near	(o)	31.4	-0.3	near	(a2)	317.0	0.3	far	(1a)
16.9	0.8	near	(o)	31.4	0.3	tangent	(a2)	320.2	0.8	near	(o)
17.0	0.8	near	(o)	31.6	0.1	near	(a1)	321.1	-0.5	near	(o)
17.0	0.9	near	(a2)	31.8	1.5	near	(o)	322.2	0.6	near	(a1)
18.1	-0.3	near	(a2)	32.2	0.1	far	(a1)	324.2	0.1	near	(o)
18.2	-0.3	near	(o)	32.8	0.2	far	(a1)	326.6	0.6	near	(a1)
18.2	-0.4	near	(a2)	33.1	-0.1	tangent	(a1)	326.7	0.6	near	(o)
18.3	-0.4	near	(a2)	33.4	-0.0	far	(a1)	327.3	-0.6	near	(a1)
18.3	-0.3	near	(a2)	34.3	0.1	near	(a1)	327.3	-0.5	near	(o)
18.3	1.9	near	(a2)	34.9	-0.0	near	(a1)	328.0	-0.1	near	(o)
18.7	2.0	near	(o)	35.1	-1.5	near	(a2)	328.3	0.4	far	(a1)
18.9	-0.4	near	(o)	35.2	-1.8	near	(a2)	328.6	-0.5	near	(o)
18.9	-0.5	near	(a2)	35.3	-1.8	near	(a2)	330.9	-0.4	near	(a1)
19.0	-0.0	near	(a2)	35.6	-0.5	near	(a1)	331.3	-0.3	near	(a1)
19.1	-0.3	near	(a2)	35.6	-0.0	far	(a1)	331.5	-0.1	far	(a1)
19.6	-0.2	near	(a2)	35.6	0.1	far	(a1)	332.8	-1.4	near	(o)
19.6	-0.1	near	(a2)	35.7	-0.0	near	(a2)	332.8	-0.6	near	(o)
19.7	-0.1	near	(a2)	36.3	-1.7	near	(o)	333.0	-0.4	far	(a1)
21.0	0.1	far	(a2)	36.5	-0.2	far	(a1)	333.1	-0.4	near	(o)
21.9	0.0	near	(o)	37.4	-0.2	far	(a2)	333.3	-0.4	near	(o)
22.8	-0.5	far	(a2)	37.4	-0.1	far	(a1)	333.6	-0.2	near	(a1)
22.9	-0.3	far	(a2)	37.4	-0.0	far	(a1)	336.4	-0.2	near	(o)
22.9	0.7	near	(o)	37.5	-0.1	far	(a1)	336.5	-1.5	near	(a1)
23.0	-0.4	far	(a2)	37.6	-0.1	far	(a1)	336.8	0.0	far	(a1)
23.1	0.6	near	(o)	37.7	-0.1	far	(a1)	337.1	-0.2	far	(a1)
23.4	-0.2	tangent	(a2)	37.8	-0.2	far	(a1)	337.9	-0.5	near	(a1)
23.5	-0.0	far	(a2)	37.9	-0.4	far	(a1)	338.9	0.6	near	(a1)
23.7	0.2	tangent	(a2)	38.1	-0.0	far	(a1)	340.8	-1.0	near	(a1)
23.9	-0.1	far	(a2)	39.9	-1.3	near	(o)	345.4	-0.9	near	(a1)
24.0	0.2	far	(a2)	40.5	2.5	near	(o)	345.4	1.4	near	(a1)
24.2	-0.1	far	(a2)	41.1	-0.2	far	(a1)	348.2	-1.0	near	(o)
24.4	0.1	tangent	(a2)	41.2	0.4	near	(a1)	348.7	-1.0	near	(o)
24.5	0.2	tangent	(a2)	41.5	0.0	far	(a1)	350.5	1.0	near	(o)
24.5	0.5	tangent	(a2)	42.1	-0.6	near	(a1)	351.6	-1.3	near	(o)
24.7	-0.2	tangent	(a2)	42.4	-0.3	far	(a1)				
24.7	-0.1	near	(o)	42.6	-0.1	near	(a1)				
24.8	0.1	tangent	(a1)	43.9	-0.8	far	(a1)				

#### 4.1 The luminosity-physical diameter correlation

A rough proportionality between luminosity and linear diameter is expected based on the following argument. The luminosity is proportional to the product of the emission measure (which is proportional to the linear diameter) with the square of the angular size. But, for our sample, the distribution of angular sizes has a dispersion of only  $6'$  which is small enough not to swamp the correlation with the emission measure.

In order to verify the correlation, we have selected from the catalog by Paladini et al. (2003) the HII regions with flux densities,  $S_\nu$ , and angular diameters,  $\theta$ , measured with the same instrument as well as with an unambiguous determination of the distance,  $D$ , from the Sun. We have 57 such sources with measurements at 2.7 GHz and 190 with measurements at 5 GHz. At both frequencies we find a highly significant correlation between the luminosity  $L_\nu = 4\pi D^2 S_\nu$  and linear diameter (see Fig. 5). The Pearson correlation coefficients are 0.54 (corresponding to a probability  $p \simeq 10^{-5}$  that the correlation is occurring by chance) at 2.7 GHz, and 0.56 ( $p \simeq 10^{-17}$ ) at 5 GHz.

On the other hand, we should worry about the possibility that the correlation is an artifact arising through the dependence of luminosity on  $D^2$  while the linear diameter is proportional to  $D$ . To check if this can be the case, we have computed the partial correlation coefficient between the two quantities, i.e. the correlation at constant  $D$ . For the combined sample of  $190 + 57$  sources (extrapolating to 5 GHz the 2.7 GHz fluxes with a spectral index of  $-0.1$ ,  $S \propto \nu^{-0.1}$ , as appropriate for optically thin free-free emission) we find a partial correlation coefficient of 0.37 for which  $p \simeq 10^{-8}$ . The correlation is therefore clearly physically significant. This issue will be further discussed in Sect. 5.

Assuming a linear relationship between  $\log L_\nu$  (in erg/s) and  $\log d$  (in pc):

$$\log L_\nu = a + b \times \log d \quad (6)$$

a least square fit yields  $a = 31.9$ ,  $b = 1.05$  at 2.7 GHz and  $a = 32.4$ ,  $b = 0.86$  at 5 GHz. Combining the two samples, we obtain  $a = 32.1$ ,  $b = 0.88$  at 5 GHz.

The solar distance  $D$  can then be estimated as:

$$D = 10^{\frac{a}{2-b}} \left(\frac{\theta}{1''}\right)^{\frac{b}{2-b}} \left(\frac{\nu}{1GHz}\right)^{\frac{-1}{2-b}} \left(\frac{S}{1Jy}\right)^{\frac{-1}{2-b}} \text{ kpc} \quad (7)$$

Although the dispersion around the above relationship is too large to make it a good distance indicator for individual sources, it allows us to discriminate in a statistical sense among the “near” and “far” solutions. To test the reliability of this approach we have applied it to the 177 sources for which the distance degeneracy has been broken using complementary data. We find that the fractions of “near” ( $\simeq 65\%$ ) and “far” ( $\simeq 35\%$ ) distances are correctly reproduced although the correct distance is assigned to only  $\simeq 60\%$  of individual sources.

We have homogeneous measurements of flux densities and of angular diameters at either 2.7 or 5 GHz for 256 out of the 281 HII regions with distance degeneracy. To these sources we apply Eq. (7). We find that 100 ( $\sim 40\%$ ) objects are assigned to the “near” solution and 155 ( $\sim 60\%$ ) to the “far” solution.

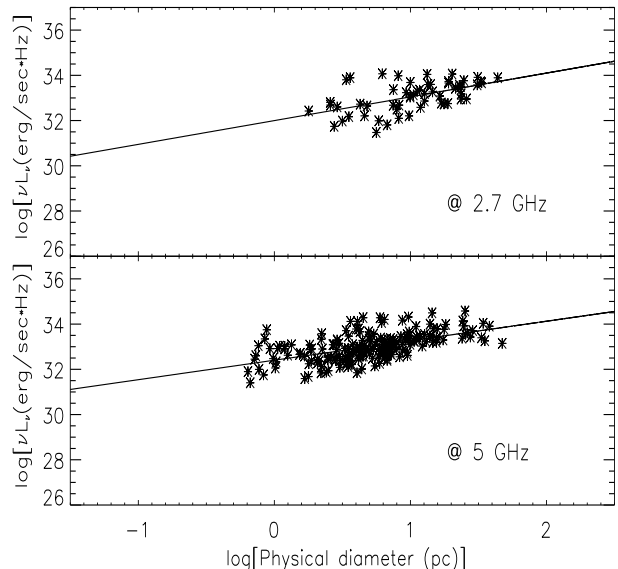


**Figure 5.** Luminosity-physical diameter correlation at 2.7 (57 sources) and 5 GHz (190 sources) for HII regions with unambiguous distances.

**Table 3.** Fractions of near (N), far (F), and tangent (T) solutions resulting from absorption data. The last column shows the number of sources of the catalog whose distance ambiguity is resolved through listed HI absorption data.

		N (%)	F (%)	T (%)	N
HI	Kuchar & Bania (1994)	20	72	8	40
	Caswell et al. (1975)	67	28	5	18
	Kerr & Knapp (1970)	55	45	-	9
H <sub>2</sub> CO	Wilson (1980)	44	37	19	84

#### 4.2 Distance degeneracy and properties of the sample

We will now consider the implications of breaking the distance ambiguity on the properties of the HII regions lying within the solar circle ( $R < R_0$ ). The considerations will include the distributions of radial distance from the Sun, the physical diameter and the source luminosity.

The distribution of distances from the Sun from different samples with unambiguous distances are shown in Fig. 6(a). The dashed line is for the 177 sources with  $R < R_0$  whose distance ambiguity has been resolved using the complementary data plotted in the insert. The full line is the sum of these 177 sources plus the 117 sources at  $R > R_0$  with unambiguous kinematic distances.

Fig. 6(b) shows the distributions of sources whose near/far degeneracy has been resolved using the luminosity-diameter relationship. It can be seen that the number of sources reaches a first peak at 3-5 kpc from the Sun followed by a minimum at 6-9 kpc and a second peak at 10-14 kpc. The minimum corresponds to distances from the Sun which include the Galactic centre region where there is a deficit of detected sources.

The distribution of sources in Fig. 6(a) with  $R < R_0$  (dashed line) shows a strong deficit in the range 12-14 kpc

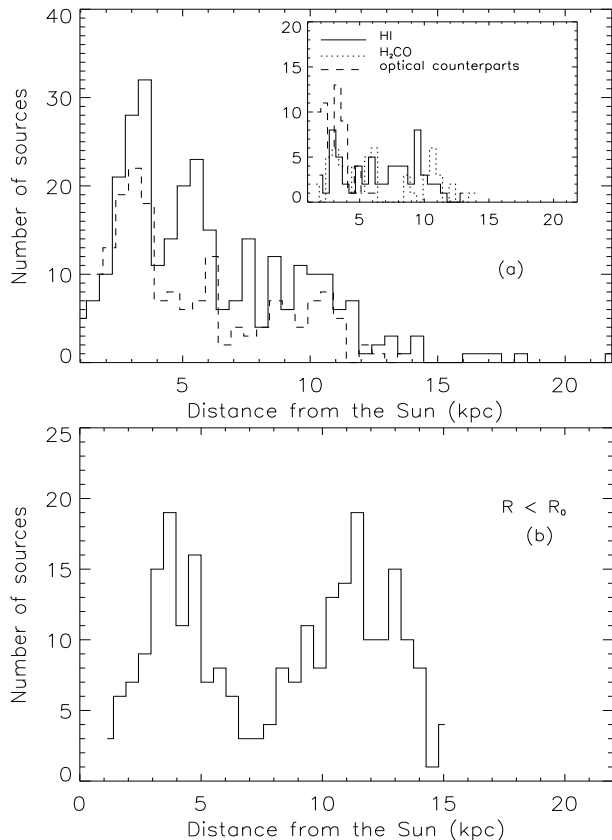


**Figure 6.** Distributions of solar distances for HII regions. The top panel shows the distribution of all 294 sources with unambiguous distance estimates (solid histogram) and of the subset of 177 sources whose near/far degeneracy was broken by complementary data (dashed). The insert details the distributions of the various kinds of complementary data. Panel (b) shows the distribution of 256 sources with near/far degeneracy resolved using the luminosity-diameter relationship.

compared with Fig. 6(b). There are a number of contributing factors. Those sources with optical counterparts are preferentially nearby because of obscuration at larger distances. In addition, it is more difficult to measure accurate absorption spectra for sources at lower flux densities; these will again be preferentially at larger distances. Table 3 illustrates this situation. The deeper survey by Kuchar & Bania (1994) shows a near to far number ratio 20:72; while the less deep survey by Caswell et al. (1975), Kerr & Knapp (1970) and Wilson (1980) have a majority of sources at the near distance.

We now turn to the distribution of linear diameters deduced from the application of our technique of resolving the distance ambiguity. Low diameter sources are somewhat under-represented in Fig. 7(b), since objects in this sample are on average at greater distances as seen in Fig. 6(b). Fig. 8 shows the 2.7 GHz luminosity distribution for the same three samples of sources as in Fig. 7. The 256 sources (Fig. 8(b)) whose distance ambiguity is broken by the use of Eq. (7) have higher intrinsic luminosities than the other two samples. Again this is because of their greater average distances for similar flux density and angular size distributions.

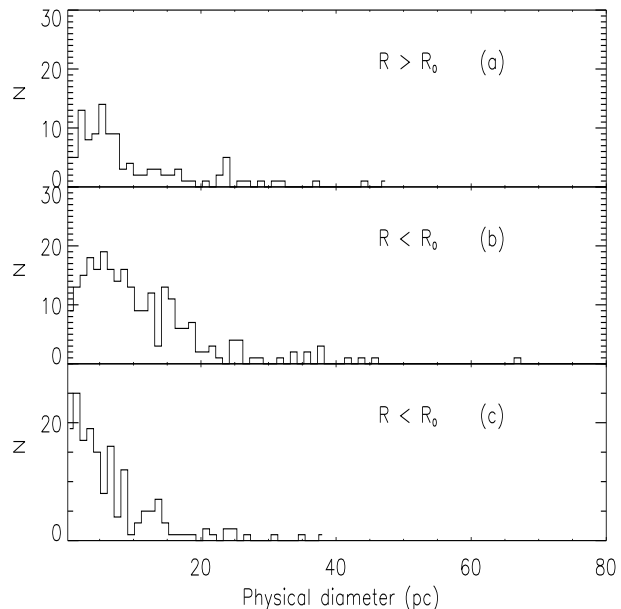


**Figure 7.** Distributions of linear diameters. Panel (a): 117 sources with unique solutions for solar distances; panel (b): 256 sources with near/far degeneracy resolved using the luminosity-diameter relationship; panel (c): 177 sources with near/far degeneracy resolved using auxiliary data.

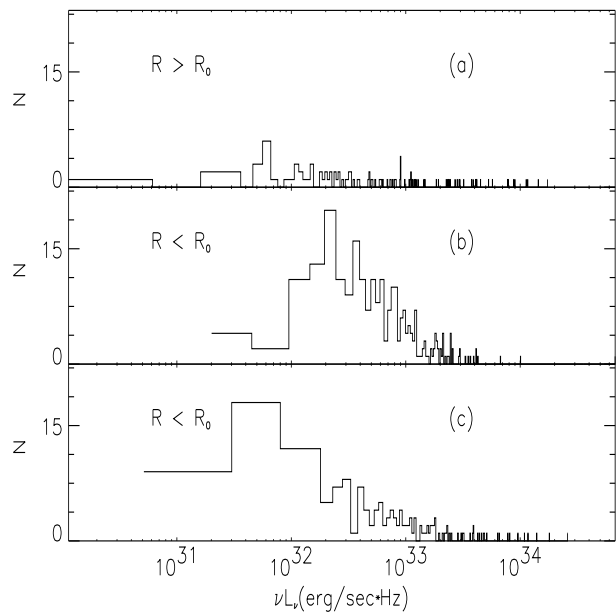


**Figure 8.** Distributions of 2.7 GHz luminosities. Panel (a): 117 sources with unique solutions for solar distances; panel (b): 256 sources with near/far degeneracy resolved using the luminosity-diameter relationship; panel (c): 177 sources with near/far degeneracy resolved using auxiliary data.

### 4.3 The $z$ -distribution of Galactic HII regions

We take all 550 HII regions with distance determination and estimate their  $z$  distances from the Galactic plane using the expression:

$$z = (D \times \sin(b)) \times 10^3 \quad (8)$$

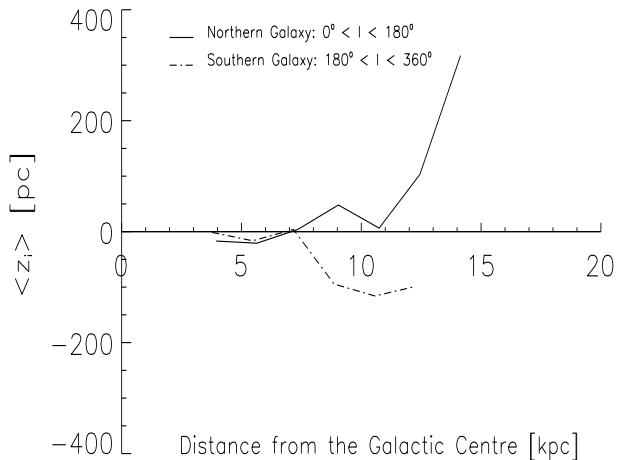


**Figure 9.** Variation of bin-averaged  $z$  with distance from the Galactic centre,  $R$ .

where  $z$  is in pc, and the distance  $D$  from the Sun is in kpc. For the Northern (quadrants I and II;  $0^\circ \leq l \leq 180^\circ$ ) and the Southern (quadrants III and IV;  $180^\circ \leq l \leq 360^\circ$ ) Galaxy, we have binned the galactocentric distances,  $R$ , into annuli  $0.2R_0$  wide. Fig. 9 shows the mean of the  $z$ -distribution,  $\langle z_i \rangle$ , where  $i$  is the index of the bin. The increasing  $\langle z_i \rangle$  with  $R$  in quadrants I and II and a corresponding decrease in quadrants III and IV clearly show the warp of the Galactic plane well known from HI and CO studies, although of smaller magnitude (see, for example, Burton 1988).

In order to investigate the thickening of the HII region layer with  $R$ , we have also computed, for each bin, the width  $\sigma_i$  of the  $z$ -distribution:

$$\sigma_i = \left[ \sum_{j=1}^N (z_j - \langle z_i \rangle)^2 \right]^{\frac{1}{2}} \quad (9)$$

where  $N$  is the number of sources in the  $i$ -bin (see Table 4). The uncertainty on  $\sigma$  is dominated by the sampling error, that we have estimated following Danese et al. (1980), on the assumption of an underlying Gaussian distribution. The result is illustrated in Fig. 10 for all 550 sources with distances and shows that on both sides of the Galaxy, the HII region layer thickens with increasing  $R$ . A similar effect is found for the distribution of OB stars by Bronfman et al. (2000) and for the distribution of molecular gas, based on the data from Cohen et al. (1986), Grabelsky et al. (1987), May et al. (1988) and Digel (1991), as reported in Bronfman et al. (2000).

For  $R < R_0$ , the width of the  $z$ -distribution (Fig. 10) is almost constant. Table 5 gives the azimuthally averaged values of  $\sigma$  for the combined Northern and Southern data sets. The best-determined distances give  $\sigma \simeq 39.3$  pc; when the data for HII regions with distances relying on Eq. (7) are included,  $\sigma \simeq 52$  pc. These values are similar to the values  $\sigma = 32$  pc derived for dust-embedded OB stars (Bronfman et al. 2000) and  $\sigma = 51$  pc for the  $H_2$  layer (Bronfman et al. 1988). The HI (Malhotra 1995; Binney & Merrifield 1998) layer is wider by a factor of about 2. Pulsar dispersion measurements indicate a thin disk of ionized hydrogen with  $\sigma = 70$  pc (Reynolds 1991).

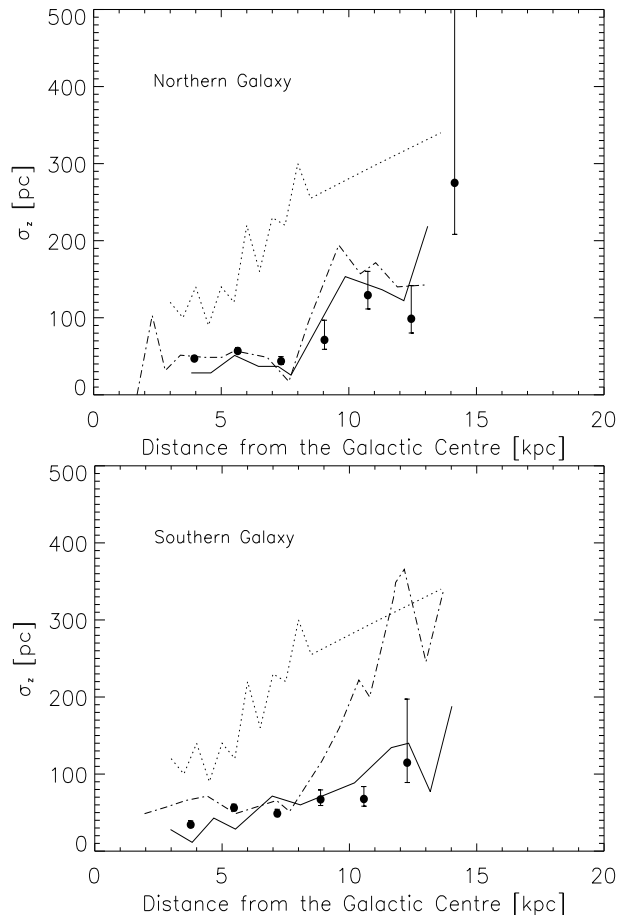


**Figure 10.** Azimuthally-averaged thickness in the Northern ( $0^\circ \leq l \leq 180^\circ$ ) and Southern ( $180^\circ \leq l \leq 360^\circ$ ) Galaxy (filled circles). Also shown for comparison are the UCHII layer (solid line), the  $H_2$  layer (dashed line) (both from Bronfman et al. 2000) and the HI layer (dotted line). Data are from Malhotra (1995) for  $R < R_0$  and from Binney & Merrifield (1998) for  $R > R_0$ .

The negative mean value of  $z$ ,  $\langle z \rangle$ , is consistent with the well known result that the sun lies above the plane: Reed (1997) finds  $z_\odot = 10$ –12 pc by analyzing the distribution of 12,522 OB stars.

## 5 CONCLUSIONS

We have analyzed the spatial distribution of 550 Galactic HII regions taken from the 2.7 GHz catalog of Paladini et al. (2003), exploiting the extensive database of kinematic information included in the catalog. For each source we have derived a galactocentric distance using the rotation model by Fich et al. (1989).

Distances from the Sun could be unambiguously derived for 117 sources, lying either outside the solar circle (84) or on a line-of-sight tangential to their orbit (33). A highly significant correlation between luminosity and linear diameter was found for these sources. The corresponding least-square linear relationship in the log-log plane was used to resolve, at least in a statistical sense, the distance ambiguity for an additional 256 sources. The reliability of this approach was successfully tested comparing the distributions of solar dis-

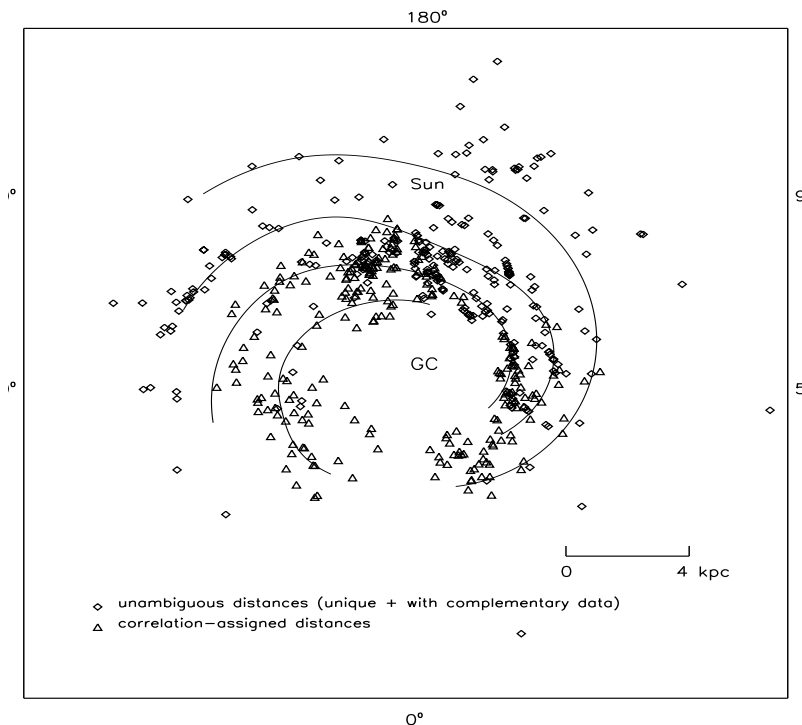


**Figure 12.** 2-D distribution of 550 HII regions from the Catalog by Paladini et al. (2003). The diamonds correspond to the 117 sources for which there is no distance ambiguity, plus the 177 sources for which the distance degeneracy was resolved thanks to auxiliary data. The triangles correspond to the 256 sources to which the luminosity-diameter correlation was applied. Also shown is the spiral arm model by Taylor & Cordes (1993). An updated version of this model is given in Cordes & Lazio 2002, 2003.

**Table 4.** Azimuthally-averaged  $\sigma_z$  for the Northern and the Southern hemisphere with sampling errors, under the assumption of an underlying Gaussian distribution. Centroids of the bins ( $R_{bin}$ ) and number of sources per bin ( $N$ ) are also shown.

$R_{bin}$ (kpc)	Northern		Southern	
	N	$\sigma_z$ (pc)	N	$\sigma_z$ (pc)
3.9	103	$47^{+3.67}_{-2.97}$	36	$34.3^{+4.9}_{-3.5}$
5.6	124	$56.9^{+4}_{-3.3}$	96	$56.2^{+4.6}_{-3.7}$
7.3	41	$43.6^{+5.9}_{-4.2}$	57	$48.8^{+5.3}_{-4.0}$
9.0	10	$71.2^{+25.5}_{-12.2}$	24	$67.1^{+12.3}_{-7.9}$
10.7	19	$129.3^{+30.8}_{-17.9}$	15	$67.6^{+16.1}_{-9.4}$
12.4	8	$98.7^{+43}_{-18.5}$	5	$114.7^{+82.5}_{-25.7}$
14.1	4	$275^{+270}_{-66}$	-	-

**Table 5.** Width  $\sigma$  and mean,  $\langle z \rangle$ , of the  $z$ -distribution within the solar circle. The results in the first column use sources with unique solutions (u) plus sources whose distance degeneracy was resolved with auxiliary data (aux) or with the luminosity-diameter correlation (assign). In the second column, the last group (assign) of sources is not included.

$\sigma$ (pc)	$\sigma$ (pc)	$\langle z \rangle$ (pc)
u+aux+assign	u+aux	
52	-	-11.3
-	39.3	-7.3

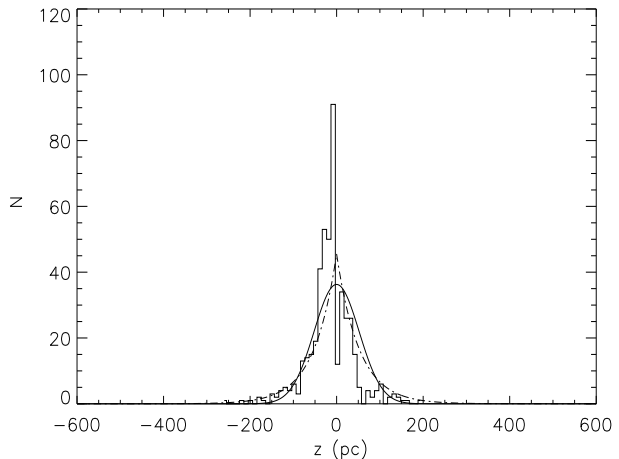


**Figure 11.**  $z$ -distribution of the 456 sources at  $R < R_0$  whose solar distance is either unambiguous or assigned through the luminosity-diameter correlation. Overlaid are a gaussian (solid line) and exponential curve (dashed line) with  $\sigma$  taken equal to 52 pc (see Table 5) and normalized to the number of plotted sources.

tances, linear diameters and luminosities so obtained with those of sources with unambiguous distances.

An analysis of the  $z$ -distribution of HII regions shows:

- (i) an increase of the mean value of  $|z|$  with  $R$ , for  $R > R_0$ , reflecting the shape of the warp;
- (ii) a corresponding increase of the width of the distribution as a function of  $R$ , comparable to what is seen for



the OB stars (Bronfman et al. 2000) and the molecular gas distribution (Cohen et al. 1986; Grabelsky et al. 1987; May et al. 1988; Digel 1991);

(iii) an azimuthally-averaged thickness of the HII region layer within the solar circle similar to that of OB stars (Bronfman et al. 2000) but narrower than those of the diffuse HII and HI (Reynolds 1991).

To check to what extent the above results depend on the adopted linear diameter–luminosity correlation, we have repeated the analysis adopting the extreme assumption that the two quantities are totally independent. In this case we have used the mean linear diameter ( $\bar{d} = 7.6$  pc) of sources with known solar distance as a distance indicator. The results for  $R > R_0$  (and, in particular, the increase of  $| < z > |$  and the thickening of the  $z$ -width with increasing  $R$ ) are obviously unchanged since objects outside the solar circle are unaffected by the distance degeneracy. For  $R < R_0$  we find  $\sigma = 51.4$  pc,  $< z > = -7.2$  pc, not significantly different from the values found using the correlation (see Table 5).

Also, we confirm, for a much larger sample, the positive gradient of electron temperature with galactocentric distance discovered in previously published works.

The 2-D distribution within the Galactic plane of HII regions having distances determined in the present study is shown in Fig. 12. The HII regions show spiral-like structures, in acceptable agreement with the spiral arms delineated by Taylor & Cordes (1993, hereafter TC93). This fact is partly expected due to the fact that the skeleton model of the arm shapes in TC93 is derived from the map published in Georgelin & Georgelin (1976), built on the basis of velocity data from Reifenstein et al. (1970) and Wilson et al. (1970) complemented by the information contained in Downes et al. (1980) and Caswell & Haynes (1987). However, our analysis exploits data not available for the TC93 analysis (see Table 1) and makes use of a different rotation curve. From this point of view, the agreement with the TC93 model is not a trivial result. A more detailed study of the spiral arm structure is beyond the goal of the current work and it will be presented in a forthcoming paper.

## ACKNOWLEDGMENTS

R. Paladini thanks all the staff at the Jodrell Bank Observatory for their hospitality and acknowledges financial support from a Marie Curie Training Site Fellowship. We are grateful to the referee for constructive comments. Work supported in part by ASI and MIUR.

## REFERENCES

Binney, J. & Merrifield M., 1998, *Galactic Astronomy*, Princeton Series in Astrophysics, Princeton University Press  
 Blitz L., 1979, APJ, 231, 115  
 Blitz L., Fich, M. & Stark A. A., 1982, ApJS, 49, 183  
 Brand J. & Blitz L., 1993, A&A, 275, 67  
 Bronfman L., Cohen R. S., Alvarez H., May J., Thaddeus P., 1988, ApJ, 324, 248  
 Bronfman L., Casassus S., May J., Nyman L.-A., 2000, A&A, 358, 521  
 Burton W. B., *Galactic and Extragalactic Radio Astronomy*, ed. Verhuur, G. L., & Kellermann, K. I., Springer-Verlag, 1988

Caswell J. L., Murray J. D., Roger R. S., Cole D. J., Cooke, D. J., 1975, A&A, 45, 239  
 Caswell J. L. & Haynes R. F. 1987, A&A, 171, 261  
 Clemens D. P., 1985, ApJ, 295, 422  
 Clemens D. P., Danders D. B., Scoville N. Z., 1988, ApJ, 327, 139  
 Churchwell E., Smith L. F., Mathis J., Mezger P. G., Huchtmeier W., 1978, A&A, 70, 719  
 Cohen R. S., Dame T. M., Thaddeus P., 1986, ApJS, 60, 695  
 Condon J.J., 1974, ApJ, 188, 279  
 Cordes J. M. & Lazio T. J. W., preprint(astro-ph/0207156)  
 Cordes J. M. & Lazio T. J. W., preprint(astro-ph/0301598)  
 Danese L., de Zotti G., di Tullio G., 1980, A&A, 82, 322  
 Dickey J. M. & Lockman F. J., 1990, ARA&A, 28, 215  
 Digel S. W., 1991, PhD Thesis, Harvard University  
 Downes D., Wilson T. L., Bieging L., Wink J. 1980, A&AS, 40, 379  
 Fich M., Blitz L., ApJ, 1984, 279, 125  
 Fich M., Blitz L., Stark A. A., 1989, ApJ, 342, 272  
 Goss W. M. & Radhakrishnan V., 1969, AstL., 4, 199  
 Grabelsky D. A., Cohen R. S., Bronfman L., Thaddeus P., May J., 1987, ApJ, 315, 122  
 Hogg D.W., 2001, ApJ, 121, 1207  
 Kerr F. J. & Knapp G. R., 1970, AuJPA, 18, 9  
 Kerr F. J. & Lynden-Bell D., 1986, MNRAS, 221, 1023  
 Kuchar T. A. & Bania T. M., 1994, ApJ, 436, 117  
 Lockman F. J., 1989, ApJS, 71, 469  
 Malhotra S., 1995, ApJ, 448, 138  
 Marsálková P. 1974, A&SS, 27, 3  
 May J., Murphy D. C., Thaddeus P., 1988, A&A, 73, 51  
 Miller J. S., 1968, ApJ, 151, 473  
 Paladini R., Burigana C., Davies R., Maino D., Bersanelli M., Cappellini B., Platania P., Smoot G., 2003, A&A, 397, 213  
 Reed B. C., 1997, PASP, 109, 1145  
 Reifenstein E. C., Wilson T. L., Burke B. F., Mezger P. G., Altenhoff W. J., 1970, A&A, 4, 357  
 Reynolds R. J., 1991, *The Interstellar Disk-Halo Connection in Galaxies*, IAU Symposium No. 144, ed. Bloemen, H., Publisher City, p. 67  
 Scheuer P.A.G., 1957, Proc. Cambridge Philos. Soc., 53, 764  
 Schmidt M., 1965, *Galactic Structure*, eds. A. Blaauw and M. Schmidt, University of Chicago Press, p. 513  
 Sharpless S. 1959, ApJS, 4, 257S  
 Shaver P. A., Retallack D. S., Wamsteker W., Danks, A. C., 1981, A&A, 102, 225  
 Shaver P. A., McGee R. X., Newton L. M., Danks A. C., Pottasch S. R., 1983, MNRAS, 204, 53  
 Stark A. A. & Brand J., 1989, ApJ, 339, 763  
 Taylor J. H. & Cordes J. M., 1993, ApJ, 411, 674  
 Vallée J. P., 1995, ApJ, 454, 119  
 Wilson T. L., Mezger P. G., Gardner F. F., Milne D. K., 1970, A&A, 6, 364  
 Wilson T. L., 1980, *Radio recombination lines*, ed. Shaver P. A., Reidel, Dordrecht, p. 205  
 Wink J. E., Altenhoff W. J., Mezger P. G. 1982, A&A, 108, 227  
 Wink J. E., Wilson T. L., Bieging J. H. 1983, A&A, 127, 211